Int. J. Electrochem. Sci., 16 **(2021)** Article ID: 210715, doi: 10.20964/2021.07.43

International Journal of
ELECTROCHEMICAL
SCIENCE
www.electrochemsci.org

A Facile Fabrication of Fe_3O_4/polypyrrole/functionalized Carbon Nanotubes Composites for Photocatalytic Degradation of Contaminants from Wastewater

Bangjun Han[*], *Ruifeng Wang, Xingya Wei, Renzheng Gu*

School of Civil and Transportation Engineering, Shanghai Urban Construction Vocational College, 200438 Shanghai, P. R. China
[*]E-mail: hanbangjun@succ.edu.cn

Received: 3 March 2021/ *Accepted:* 19 April 2021 / *Published:* 31 May 2021

This work was conducted on fabrication of Fe_3O_4/polypyrrole/functionalized carbon nanotubes (Fe_3O_4/PPy@f-MWCNTs) composite as photocatalyst for degradation of Bisphenol A from industrial wastewater. The composite was synthesized via a situ polymerization process. The structural analyses of Fe_3O_4/PPy@f-MWCNTs using SEM and XRD showed that polypyrrole particles and Fe_3O_4 spheres in cubic spinel crystal structure were uniformly decorated on the CNTs network. The optical study showed that the lower band gap of Fe_3O_4/PPy@f-MWCNTs toward PPy@f-MWCNTs can related to the presence of more photoactivated site in sunlight region and cost-effective photocatalytic performance of Fe_3O_4/PPy@f-MWCNTs. Moreover, the electrochemical studies illustrated the higher effective surface area of Fe_3O_4/PPy@f-MWCNTs that indicated the higher photocatalytic active sites and consequently higher photocatalytic performance of composite. The photocatalytic studies of Fe_3O_4/PPy@f-MWCNTs revealed that the degradation rate under simulated sunlight was enhanced than that under UV light illumination. Moreover, the complete degradation of BPA was obtained after 15, 25, 35, 47 and 65 minutes simulated sunlight irradiation for 10, 20, 50 and 100 mM of initial concentration of BPA, respectively. These results show that the prepared photocatalyst can be reliable for the degradation of BPA in wastewater samples.

Keywords: Fe_3O_4 nanoparticles;Polypyrrole; Functionalized carbon nanotubes; Photocatalyst; Bisphenol A; Simulated sunlight

1. INTRODUCTION

Bisphenol A (BPA, 4,4'-isopropylidenediphenol) as organic compound is white to light brown flakes or powder that is an important commercial chemical to synthesis of epoxy, polycarbonate, phenoxy, polysulfone and polyester resins [1]. Moreover, it is also used in thermal papers, food packaging, flame, rubber, paints and coatings industries [2, 3]. Researchers have been shown that BPA can mimic the effects of natural estrogen and antagonize estrogen, and be able to trigger estrogenic

pathways in the body. It causes skin irritation and rash in some people; this may be a side effect or an allergic reaction. There is concern that BPA affects the brain, behavior and prostate gland in fetuses, damage to bone marrow cells and blood components [4].

Therefore, these concerns have been raised about the increasing use of BPA in food packaging product industries [5]. When the beverage bottles and coated water pipes have been heated at high temperatures, BPA can leach from these products. Studies show application of BPA at the current levels as main chemical composition of polycarbonate plastic in fabrication of food packaging products such as beverage containers and food and beverage can liners is safe for adults [6, 7]. However, in order to quell concerns, the United States' Food and Drug Administration (FDA) banned the use of BPA in baby bottles, children's sippy cups and infant formula cans.

Therefore, worldwide concerns have been caused to development of determination and degradation techniques of BPA with physical and chemical methods such as filtration, electroflotation, electrocoagulation, electrochemical oxidation and photodegradation [5-8]. Among these methods, photodegradation as semiconductor nanoparticle-assisted photocatalytic process is cost-effective and promising technique that it relies on oxidation of pollutants under UV and visible light irradiations which related to band gap value of semiconductor and its photoactivation in UV and visible region [9]. Accordingly, fabrication of the durable photocatalyst and band gap engineering with nanostructure materials provide an opportunity for enhancement of degradation rate and decrease the recombination of photogenerated electron-holes [10-13]. For example, Wang et al. [14] synthesized Mg doped ZnOnanotapers for degradation BPA under UV and visible light irradiations. They showed that the band gap value was decreased for doped ZnO because of the presence of Mg^{2+} in ZnO lattice that improved the charge separation. Thus, this study was conducted on fabrication of Fe_3O_4/PPy@f-MWCNTs composites for photocatalytic degradation of BPA from wastewater.

2. EXPERIMENT

PPy@f-MWCNTs and Fe_3O_4/PPy@f-MWCNTs composites were synthesized through a situ polymerization process [15]. All solutions were prepared using deionized water. The 1g MWCNTs (99%, Xuzhou Jiechuang New Material Technology Co., Ltd., China) were purified and functionalized through ultrasonically dispersing in mixture of 10 ml of1 M nitric acid (68%, Qingdao HiseaChem Co., Ltd., China) and 10 ml of 1 M sulfuric acid (98%, Xilong Scientific Co., Ltd., China) at40°C for 10 hours to formation carboxyl groups at the of defects sites on CNTs surface [16]. Then, functionalized MWCNTs were ultrasonically washed with deionized water for 15 minutes and dispersed in 50 ml ethanol (96%, Shandong Kawah Oils Co., Ltd., China). For preparation of PPy@f-MWCNTs, 5 ml Pyrrole (98%, Sigma-Aldrich), 2ml of 1 M $HClO_4$ (99.99 %, Sigma-Aldrich) and 2ml of ammonium persulfate (98.5%, Shanghai Sky Chem Industrial Co., Ltd., China) solution were added to dispersed MWCNTs suspension under magnetic stirrer for10 hours to perform the polymerization reaction. For reparation of Fe_3O_4/PPy@f-MWCNTs composite, 5 ml 10mM of $FeCl_3 \cdot 6H_2O$ (99%, Xilong Scientific Co., Ltd., China) was added into the prepared mixture under ultrasonic dispersion for

8 hours. Finally, 5ml acetone (99%, Xilong Scientific Co., Ltd., China) was added to the polymerized mixture to terminate the reaction. The mixture was dried at room temperature.

The scanning electron microscopy (SEM,LEO. 1430VP, Germany) was used to study the morphology of prepared composites. Crystal structures of the composites were studied by powder X-ray diffraction (XRD, Bruker D 8 Advance) operating with Cu-Kα X-rays of wavelength λ = 1.5406 Å at 40 kV and 40 mA. The optical absorption spectra were obtained via UV–vis–NIR scanning spectrophotometer (Shimadzu UV-3101PC, Japan). Electrochemical studied were conducted on via cyclic voltammetry (CV) measurements with Metrohm Autolab instruments (Autolab model 302N, Eco Chemie B.V.A) at a scan rate of 100 mV/sunder applied potential range from -0.3 to 0.7 mV in a three electrode configuration which contained prepared films as working electrode, Ag/AgCl as reference and Pt mesh as counter electrode. The electrolytes of CV experiments was of 0.1 M phosphate buffer solution (PBS) containing 0.1 M KCl (99%, Lianyungang KANDS Chemical Co., Ltd., China) and 1 mM $K_3Fe[CN]_6$ (99. 5%, Xilong Scientific Co., Ltd., China). 0.1 M PBS was prepared fromNa_2HPO_4 (99.0%, Xilong Scientific Co., Ltd., China).

The photodegradation measurements were performed in a photochemical reactor which contained the cylindrical glass with a quartz immersion well. The UV (300W medium-pressure mercury lamp) and simulated sunlight (350 W xenon lamp) as light sources were placed in the quartz immersion well. All photodegradation measurements of solutions were carried out under common mixing via a magnetic stirrer at the bottom of the photochemical reactor. Before irradiation, to reach the adsorption equilibrium, the prepared photocatalyst were kept in the dark in BPA solution for 30 minutes. The concentration of the irradiated solutions during the photodegradation was determined by UV–Visible spectrophotometer (Shimadzu UV-3101PC, Japan). The degradation efficiency (%) of BPA was measured through the recorded absorption peak intensity as following equation [17]:

$$\text{Degradation efficiency} = \frac{I_0 - I_t}{I_0} \times 100 = \frac{C_0 - C_t}{C_0} \times 100 \qquad (1)$$

where, I_0 presents the initial absorption peak intensity of BPA solution and I_t is absorption peak intensity of BPA solution after irradiation. C_0 is the initial concentration of BPA solution and C_t is concentration of BPA solution after irradiation. The applicability of the photocatalyst was evaluated in a real sample of industrial wastewater of Shenzhen, China. The samples were collected after the biological treatment stage and transported to the laboratory and analyzed for physicochemical parameters according to standard techniques for the examination of water and wastewater (APHA) [18]. BPA concentration measurements were conducted by Shimadzu HPLC coupled with UV–vis detector [19]. In the HPLC method, the physicochemical parameters of wastewater are presented in Table 1.The wastewater was filtered and centrifuged at 2000 rpm for 10 minutes. The resulting supernatant was applied to prepare the 5 mM PBA solution.

Table 1. Physicochemical parameters of wastewater

Property	value
Dissolved organic carbon	20 mg l^{-1}

Chemical oxygen demand	42 mg l^{-1}
BPA	0.11 mg l^{-1}
pH	6.9
Conductivity	2.1 mS cm^{-1}

3. RESULTS and DISCUSSION

Figure 1 shows the SEM images of f-MWCNTs and Fe_3O_4/PPy@f-MWCNTs composite.

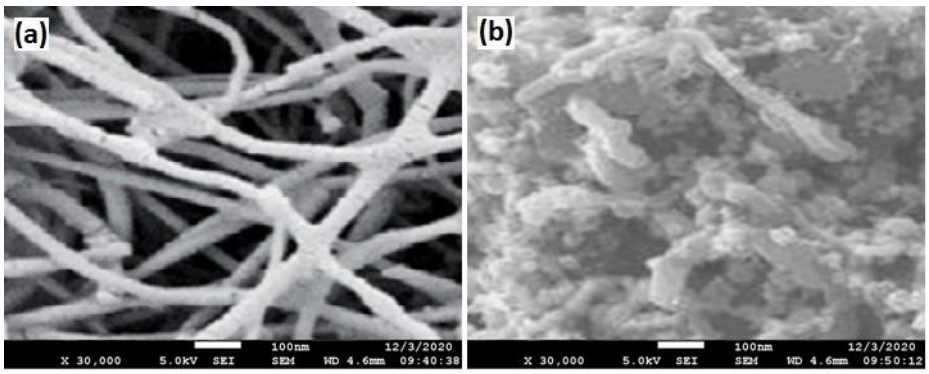

Figure 1.SEM images of (a) f-MWCNTs, (b) Fe_3O_4/PPy@f-MWCNTs composites.

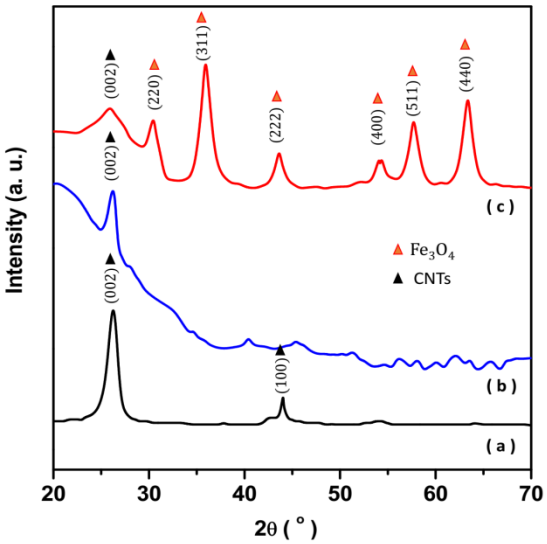

Figure 2.XRD patterns of (a) f-MWCNTs, (b) PPy@f-MWCNTs and (c) Fe_3O_4/PPy@f-MWCNTs composites.

As observed from Figure 1a, the purified and f-MWCNTs network is synthesized in smooth nanotube structure with average diameter and length of 50 nm and 4 µm, respectively. The SEM image of Fe_3O_4/PPy@f-MWCNTs composite shows that Fe_3O_4 spheres are uniformly decorated in the CNTs

network (Figure 1b). It can observe the rough surface and many irregular Fe_3O_4 clusters because of the covered Fe_3O_4 nanoparticles and polypyrrole on the f-MWCNTs and generated many aggregates. Moreover, the carboxyl groups have been formed on the defects sites on the end of CNTs walls where are good sites to anchor and form clusters of polymer and Fe_3O_4 particles [20]. Therefore, the rough surface and rod-like structure of composite is observed. The high aspect ratio, higher porosity and roughness on Fe_3O_4/PPy@f-MWCNTs surface can be attributed to its higher effective surface area and greater chemical, photo and electrocatalytic active sites[21-23].

Figure 2 shows the XRD patterns of f-MWCNTs and PPy@f-MWCNTs composite. The XRD pattern of the f-MWCNTs exhibits two diffraction peaks at 26.25° and 43.98° which ascribed to formed graphite structure of MWCNTs with planes of (002) and (100), respectively (JCPDS no. 01-0646). The XRD pattern of the PPy@f-MWCNTs composite in Figure 2b reveals the CNTs diffraction peak at 26.27° on the broad shoulder due to the pyrrole intermolecular spacing and its amorphous nature [24, 25].The results indicate that pyrrole was embedded into the f-MWCNTs matrix. The XRD pattern of Fe_3O_4/PPy@f-MWCNTs in Figure 2c shows that Fe_3O_4particle on f-MWCNTs matrix phase are formed in the cubic spinel crystal structure with (220), (311), (400), (511) and (440) planes according to diffraction peaks at 30.15°, 35.66°, 43.12°, 54.10°, 57.61° and 63.11°, respectively (JCPDS card No. 19-0629). The presence of (002) plane of CNTs in XRD pattern of Fe_3O_4/PPy@f-MWCNTs is also indicated to incorporation of Fe_3O_4 on f-MWCNTs structure.

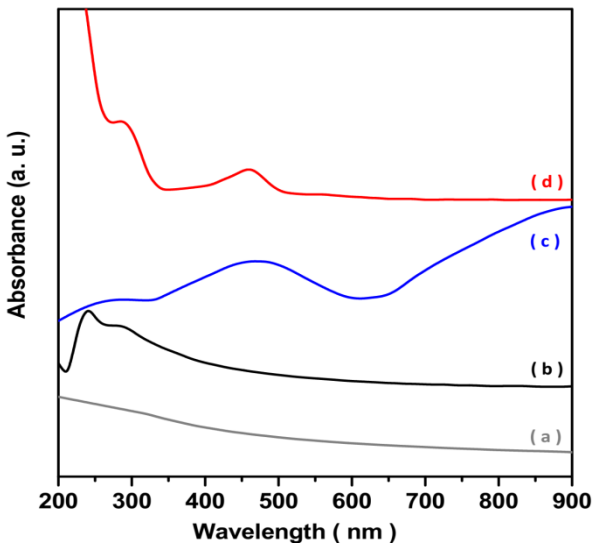

Figure 3. UV–Vis spectra of (a) MWCNTs, (b) f-MWCNTs, (c) PPy@f-MWCNTs and (d)Fe_3O_4/PPy@f-MWCNTs composites

UV–Vis spectra of MWCNTs, f-MWCNTs and PPy@f-MWCNTs composite are shown in Figure 3. From Figure 3a, it is not observed any absorption peak for MWCNTs in the wavelength range from 300 to 900 nm that is similar to previous reports on CNTs [26]. The spectra of f-MWCNTs shows the weak peak at 269 nm which is attributed to functionalization of MWCNTs and presence of polar functional groups on MWCNTs surface walls [26]. The spectra of PPy@f-MWCNTs composite

presents the absorption peak at 271 and 467 nm which could be related to the π–π* transition of polypyrrole and transition from the valence band to the antibonding polar on state, respectively, assigned to oxidized state of pyrrole in graft copolymer and band gap energy of 2.62 eV [27, 28]. These results demonstrate the interaction between the quinoid rings of pyrrole and f-MWCNTs and this could change the polymer conformation [29]. For Fe_3O_4/PPy@f-MWCNTs, there are the absorption peaks at 280 and 490 nm which correspond to π–π* transition of polypyrrole and band gap energy is 2.53 eV, respectively [30]. Therefore, the lower band gap can be related to presence of the more photoactivated site in the sunlight region and cost-effective photocatalytic performance of Fe_3O_4/PPy@f-MWCNTs.

The electrochemical characterizations of films were investigated through the CV measurements in 0.1 M PBS (pH 7.0) containing 0.1 M KCl and 1 mM $K_3Fe[CN]_6$ as redox active species at a scan rate of 100 mV/s. As seen from Figure 4, All electrodes show a pair of reversible redox peaks which are associated with the direct electron transfer. The highest redox peak current is observed for Fe_3O_4/PPy@f-MWCNTs composite with anodic and cathodic peaks potentials at 0.26 V and 0.12 V, respectively. Moreover, the higher surrounded area by CV curve of the Fe_3O_4/PPy@f-MWCNTs electrode that f-MWCNTs, PPy@f-MWCNTs electrodes evidence to the higher effective surface area of electrodes and positive effect of the modification of the f-MWCNTs with polypyrrole and Fe_3O_4 particles which implied to larger electroactive and catalytic active site on surface of composite and high electron transfer properties[31, 32]. Therefore, the higher effective surface area can be indicated to the higher photocatalytic active sites and consequently higher photocatalytic performance of Fe_3O_4/PPy@f-MWCNTs composite that is in agreement with the results of SEM studies.

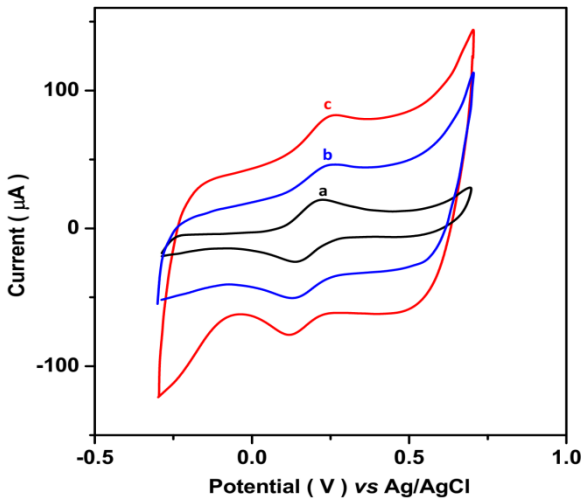

Figure 4. The CV curves of (a) f-MWCNTs, (b) PPy@f-MWCNTs and (c) Fe_3O_4/PPy@f-MWCNTs composites in 0.1 M PBS (pH 7.0) containing 0.1 M KCl and 1 mM $K_3Fe[CN]_6$ at a scan rate of 100 mV/s.

To study photocatalytic performance of prepared photocatalyst for the degradation of BPA, degradation experiments were carried out in 5 mM of BPA aqueous solution after 15 minutes UV and simulated sunlight irradiations. As observed from Figure 5, the degradation efficiencies of 2, 11, 40 and 71% are obtained in blank sample (without photocatalyst), and presence of f-MWCNTs , PPy@f-MWCNTs, Fe_3O_4/PPy@f-MWCNTs photocatalysts after 15 minutes irradiation of UV light, respectively. Many researchers have been focused to replacing UV light with sunlight for degradation of pollutants and dyes because the sunlight is around 42 to 43 % visible (400 to 700 nm), and 3 to 5% UV (below 400 nm) [33]. Therefore, the photocatalytic performance of photocatalysts was also studied under simulated sunlight excitation. As seen from Figure 5, the degradation efficiencies of 1.5, 10, 45 and 100% are obtained in blank sample and presence of f-MWCNTs, PPy@f-MWCNTs, Fe_3O_4/PPy@f-MWCNTs photocatalysts after 12 minutes irradiation of UV light, respectively. Thus, the Fe_3O_4/PPy@f-MWCNTs composite displays the excellent photodegradation ability towards BPA with higher degradation rate than other prepared film under UV and simulated sunlight irradiation. This is mainly because of existence of CNTs and Fe_3O_4 conducting particles can enhance the adsorption capacity and degradation rate of Fe_3O_4/PPy@f-MWCNTs [34]. Moreover, the complete degradation of BPA is obtained after 15simulated sunlight irradiation which implied to higher degradation rate of Fe_3O_4/PPy@f-MWCNTs in simulated sunlight than UV light illumination due to the absorption of sunlight by polypyrrole moiety. In addition, the absorption of sunlight by photoactive nonmaterials such as CNTs and PPy leads to promote the separation of photogenerated electrons and holes which play the main role in degradation activity [34]. Therefore, the following photodegradation studies were conducted on Fe_3O_4/PPy@f-MWCNTs as photocatalyst.

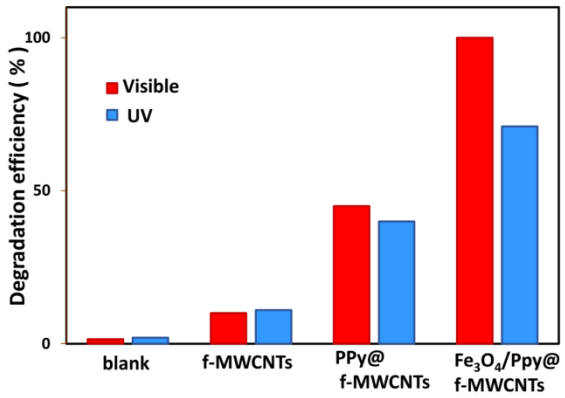

Figure 5. Degradation efficiency of blank sample, f-MWCNTs, PPy@f-MWCNTs, Fe_3O_4/PPy@f-MWCNTs in 5 mM of BPA aqueous solution (pH 6.9) after 15 minutes UV and simulated sunlight irradiations

The photodegradation of 5, 10, 20, 50 and 100 mM of BPA aqueous solution under simulated sunlight irradiation are shown in Figure 6. It is observed that the photodegradation rate is decreased with increasing the initial concentration of BPA. With increasing the initial concentration of BPA, more BPA molecules are adsorbed on the photocatalyst surface and saturate the photoactive sites [35]. So, the formation of hydroxyl radicals is reduced [35]. Furthermore, increasing the BPA molecules in

solution and near the photocatalyst surface can decrease the light path length and scatter the irradiated light [36]. The complete degradation of BPA occurred after 15, 25, 35, 47 and 65 minutes simulated sunlight irradiation for 10, 20, 50 and 100 mM of initial concentration of BPA, respectively.

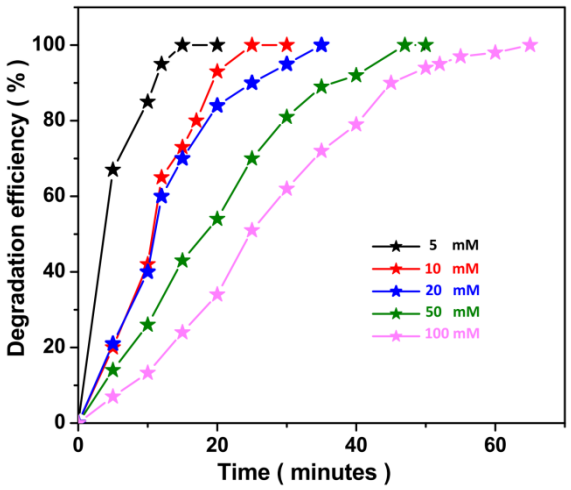

Figure 6. Variation of degradation efficiency of Fe_3O_4/PPy@f-MWCNTs vs. irradiation time for 5, 10, 20, 50 and 100 mM of BPA aqueous solution (pH 6.9) under simulated sunlight irradiation

Table 2 shows a comparison between photocatalytic activity of the Fe_3O_4/PPy@f-MWCNTs in this study and other reported photocatalyst for degradation of BPA. A seen from the Table 2, the 99.9% degradation efficiency of 100 mM BPA solution was obtained for ZnO photocatalyst after 60 minutes UV radiation, while 100% degradation efficiency is obtained for Fe_3O_4/PPy@f-MWCNTs after 65 minutes simulated sunlight radiation. Therefore, the achievement of cost-effective and rapid degradation of BPA can be a novelty of this study under sunlight radiation. By considering the initial concentration of BPA and degradation time, the prepared Fe_3O_4/PPy@f-MWCNTs shows the excellent photodegradation activity under sunlight irradiation because of synergetic effect of nanostructured Fe_3O_4 and CNTs and photoactivity of polymer.

Table 2. Comparison between photocatalytic activity of the Fe_3O_4/PPy@f-MWCNTs and other reported photocatalyst for degradation of BPA.

Photocatalyst	**Light source**	**Initial concentration of BPA (mM)**	**Degradation time (minute)**	**Degradation efficiency (%)**	**Ref.**
TiO_2 /polyurethane foam cube	UV	0.044	360	97	[37]
Mg-doped ZnOnanotapers	UV Visible	0.220	180 170	100 100	[14]
rGH-AgBr@rGO	visible light	0.28	360	100	[38]
TiO_2	UV	0.56	120	100	[39]

TiO_2/Ti	Simulated sunlight	8	180	85	[40]
rGO–P25	Sunlight	10	30	100	[41]
Palladium/ mesoporous graphite carbon nitride	Simulated sunlight	20	60	100	[42]
porous ZnO Nanoparticles	Simulated sunlight	30	60	99	[43]
rGO-ZnTi	Simulated sunlight	10	180	88.12	[44]
C-doped ZnO	UV	50	1440	100	[45]
ZnO	UV	100	60	99.9	[46]
Fe_3O_4/PPy@f-MWCNTs	Simulated sunlight	5	15	100	This work
		10	25	100	
		20	35	100	
		50	47	100	
		100	65	100	

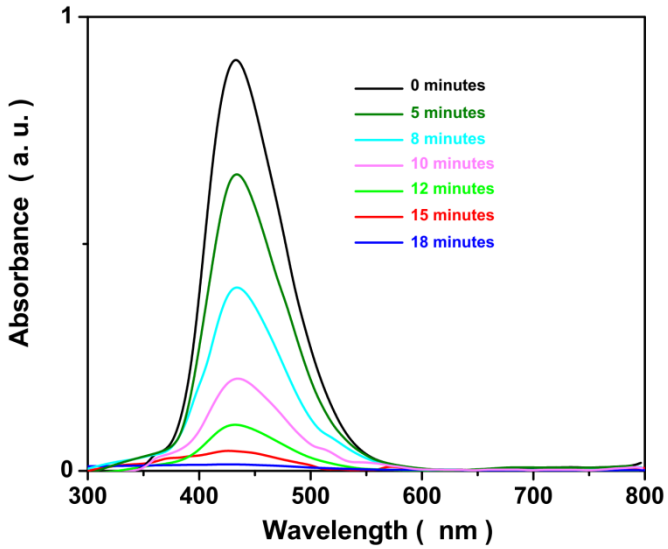

Figure 7. UV–Vis spectra of photodegradation reaction of prepared 5 mM of BPA aqueous solution (pH 6.9) from industrial wastewater respect to different irradiation times by Fe_3O_4/PPy@f-MWCNTsphotocatalyst

In order to study the applicability of the photocatalyst in real samples of industrial wastewater, the UV-visible spectrum of the photocatalytic activity of Fe_3O_4/PPy@f-MWCNTs for the degradation of BPA were studied in prepared 5 mM of BPA aqueous solution from industrial wastewater. The degradation performance is monitored by measuring the concentration of BPA under various

irradiation times. In Figure 7, the absorption peak of Fe_3O_4/PPy@f-MWCNTs photocatalyst towards the BPA is observed at 440 nm and it is decreased significantly with the increase of irradiation time which indicates to degradation of BPA. As observed, the complete degradation is obtained after 18 minutes Irradiation which is higher than that of the prepared 5 mM of BPA aqueous solution from deionized water (15 minutes). This additional time (3 minutes) could be related to presence of BPA molecules in industrial wastewater. Therefore, the prepared photocatalyst can be reliable for the degradation of BPA in wastewater samples.

4. CONCLUSION

This study was carried out for fabrication of Fe_3O_4/PPy@f-MWCNTs composite for photocatalytic degradation of Bisphenol A as contaminant from industrial wastewater. The composites were synthesized through a situ polymerization process. The structural analyses of Fe_3O_4/PPy@f-MWCNTs composite revealed that Fe_3O_4 spheres in cubic spinel crystal structure were uniformly decorated the CNTs network and Fe_3O_4/PPy@f-MWCNTs displayed the rough surface and many irregular clusters Fe_3O_4 particles because of Fe_3O_4 particles and polypyrrole were covered the f-MWCNTs and generated many aggregates. The optical study showed that the lower band gap of Fe_3O_4/PPy@f-MWCNTs toward PPy@f-MWCNTs can related to presence the more photoactivated site in sunlight region and cost-effective photocatalytic performance of Fe_3O_4/PPy@f-MWCNTs. Electrochemical studies showed the higher effective surface area of Fe_3O_4/PPy@f-MWCNTs which indicated the higher photocatalytic active sites and consequently higher photocatalytic performance of composite. The photocatalytic studies of Fe_3O_4/PPy@f-MWCNTs represented the degradation rate under simulated sunlight was enhanced than that under UV light illumination. Moreover, the complete degradation of BPA was obtained after 15, 25, 35, 47 and 65 minutes simulated sunlight irradiation for 10, 20, 50 and 100 mM of initial concentration of BPA, respectively. Finally, the study of applicability of the photocatalyst for degradation BPA showed that the prepared photocatalyst can be reliable for the degradation of BPA in wastewater samples.

References

1. Z. Pan, F. Yu, L. Li, C. Song, J. Yang, C. Wang, Y. Pan and T. Wang, *Separation and Purification Technology*, 227 (2019) 115695.
2. M.C. Dumitrascu, C. Mares, R.-C. Petca, F. Sandru, R.-I. Popescu, C. Mehedintu and A. Petca, *Oncology Letters*, 20 (2020) 1.
3. H. Karimi-Maleh, Y. Orooji, A. Ayati, S. Qanbari, B. Tanhaei, F. Karimi, M. Alizadeh, J. Rouhi, L. Fu and M. Sillanpää, *Journal of Molecular Liquids*, 329 (2021) 115062.
4. H. Inadera, *International journal of medical sciences*, 12 (2015) 926.
5. X. Chen, G. Huang and J. Wang, *Journal of Metallurgical Engineering (ME) Volume*, 2 (2013) 117570.
6. Q. Li, T. Li and Q. Wang, *International Journal of Electrochemical Science*, 15 (2020) 6759.

7. N. Abd Azis, I.M. Isa, N. Hashim, M.S. Ahmad, S. Nur, A.M. Yazid, M.I. Saidin, S.M. Si, R. Zainul and A. Ulianas, *International Journal of Electrochemical Science*, 15 (2020) 9088.
8. H. Karimi-Maleh, S. Ranjbari, B. Tanhaei, A. Ayati, Y. Orooji, M. Alizadeh, F. Karimi, S. Salmanpour, J. Rouhi and M. Sillanpää, *Environmental Research*, 195 (2021) 110809.
9. J. Rouhi, S. Kakooei, M.C. Ismail, R. Karimzadeh and M.R. Mahmood, *International Journal of Electrochemical Science*, 12 (2017) 9933.
10. R. Hassanzadeh, A. Siabi-Garjan, H. Savaloni and R. Savari, *Materials Research Express*, 6 (2019) 106429.
11. H. Savaloni and R. Savari, *Materials Chemistry and Physics*, 214 (2018) 402.
12. H. Karimi-Maleh, M. Alizadeh, Y. Orooji, F. Karimi, M. Baghayeri, J. Rouhi, S. Tajik, H. Beitollahi, S. Agarwal and V.K. Gupta, *Industrial & Engineering Chemistry Research*, 60 (2021) 816.
13. J. Rouhi, S. Kakooei, S.M. Sadeghzadeh, O. Rouhi and R. Karimzadeh, *Journal of Solid State Electrochemistry*, 24 (2020) 1599.
14. M. Wang, S. Yuan, B. Lv and H. Yang, *International Journal of Electrochemical Science*, 16
15. B. Zhang, Y. Xu, Y. Zheng, L. Dai, M. Zhang, J. Yang, Y. Chen, X. Chen and J. Zhou, *Nanoscale Research Letters*, 6 (2011) 431.
16. L. Thi Mai Hoa, *Diamond and Related Materials*, 89 (2018) 43.
17. B. Gong, P. Wu, J. Yang, X. Peng, H. Deng and G. Yin, *International Journal of Electrochemical Science*, 16 (2021) 21023.
18. A.P.H. Association, A.W.W. Association, W.P.C. Federation and W.E. Federation, *Standard methods for the examination of water and wastewater*. Vol. 2. 2005, the University of California: American Public Health Association.
19. M.E. Mutseyekwa, Ş. Doğan and S. Pirgalıoğlu, *Water Science and Technology*, 76 (2017) 2764.
20. A.H. Labulo, B.S. Martincigh, B. Omondi and V.O. Nyamori, *Journal of Materials Science*, 52 (2017) 9225.
21. J. Meng, X. Liu, C. Niu, Q. Pang, J. Li, F. Liu, Z. Liu and L. Mai, *Chemical Society Reviews*, 49 (2020) 3142.
22. H. Savaloni, E. Khani, R. Savari, F. Chahshouri and F. Placido, *Applied Physics A*, 127 (2021) 1.
23. F. Chahshouri, H. Savaloni, M. Khoramshahi and R. Savari, *3rd International Biennial Oil, Gas and Petrochemical Conference*, 1 (2020) 1.
24. I.D. Rosca, F. Watari, M. Uo and T. Akasaka, *Carbon*, 43 (2005) 3124.
25. J. Fan, M. Wan, D. Zhu, B. Chang, Z. Pan and S. Xie, *Journal of Applied Polymer Science*, 74 (1999) 2605.
26. B.K. Shrestha, R. Ahmad, S. Shrestha, C.H. Park and C.S. Kim, *Scientific Reports*, 7 (2017) 16191.
27. X. Chen, N. Yu, L. Zhang, Z. Liu, Z. Wang and Z. Chen, *RSC advances*, 5 (2015) 96888.
28. D.N. Huyen, N.T. Tung, T.D. Vinh and N.D. Thien, *Sensors (Basel, Switzerland)*, 12 (2012) 7965.
29. R. Turcu, A. Darabont, A. Nan, N. Aldea, D. Macovei, D. Bica, L. Vekas, O. Pana, M. Soran and A. Koos, *Journal of optoelectronics and advanced materials*, 8 (2006) 643.
30. J. Guo, H. Gu, H. Wei, Q. Zhang, N. Haldolaarachchige, Y. Li, D.P. Young, S. Wei and Z. Guo, *The Journal of Physical Chemistry C*, 117 (2013) 10191.
31. Y. Xia, Y. Mo, W. Meng, X. Du and C. Ma, *Polymers*, 11 (2019)
32. R. Savari, H. Savaloni, S. Abbasi and F. Placido, *Sensors and Actuators B: Chemical*, 266 (2018) 620.
33. G. Li, C. Guo, M. Yan and S. Liu, *Applied Catalysis B: Environmental*, 183 (2016) 142.
34. L. Midya, A. Chettri and S. Pal, *ACS Sustainable Chemistry & Engineering*, 7 (2019) 9416.

35. A. Garg, T. Singhania, A. Singh, S. Sharma, S. Rani, A. Neogy, S.R. Yadav, V.K. Sangal and N. Garg, *Scientific Reports*, 9 (2019) 765.
36. U.G. Akpan and B.H. Hameed, *Journal of hazardous materials*, 170 (2009) 520.
37. R. Wang, D. Ren, S. Xia, Y. Zhang and J. Zhao, *Journal of Hazardous Materials*, 169 (2009) 926.
38. F. Chen, W. An, L. Liu, Y. Liang and W. Cui, *Applied Catalysis B: Environmental*, 217 (2017) 65.
39. K. Chiang, T.M. Lim, L. Tsen and C.C. Lee, *Applied Catalysis A: General*, 261 (2004) 225.
40. V.M. Daskalaki, Z. Frontistis, D. Mantzavinos and A. Katsaounis, *Catalysis Today*, 161 (2011) 110.
41. F. Yu, X. Bai, C. Yang, L. Xu and J. Ma, *Catalysts*, 9 (2019) 607.
42. C. Chang, Y. Fu, M. Hu, C. Wang, G. Shan and L. Zhu, *Applied Catalysis B: Environmental*, 142-143 (2013) 553.
43. Y. Wang, K. Hu, Z. Yang, C. Ye, X. Li and K. Yan, *Frontiers in Bioengineering and Biotechnology*, 8 (2021)
44. S. Yang, P. Wu, M. Chen, Z. Huang, W. Li, N. Zhu and Y. Ji, *RSC Advances*, 6 (2016) 26495.
45. O. Bechambi, S. Sayadi and W. Najjar, *Journal of Industrial and Engineering Chemistry*, 32 (2015) 201.
46. R. Abo, N.-A. Kummer and B.J. Merkel, *Drinking Water Engineering and Science*, 9 (2016) 27.